CERN-TOTEM-NOTE-2013-002
13 June 2013

Geant4 simulations for the TOTEM upgrade program

F. Nemes

June 13, 2013

Contents

1 Introduction **2**

2 Geant4 simulation environment **2**
2.1 Physics list, production cuts 2
2.2 Overall description of model geometry 2
2.3 Particle generator definitions and purposes 3
2.3.1 δ-function profile 3
2.3.2 Profile based on measured rate 4

3 Single Roman Pot studies **8**
3.1 Materials and geometries of the Roman Pots 8
3.1.1 Materials 8
3.1.2 Standard Roman Pot 8
3.1.3 Cylindrical Roman Pot 10
3.2 Secondary particle production 11
3.2.1 δ-function profile 11
3.2.2 Profile based on measured rate 14
3.3 Conclusions 16

4 Multiple Roman Pot studies **17**
4.1 Secondary particle production 17
4.1.1 δ-function profile 17
4.1.2 Profile based on measured rate 18
4.2 Conclusions 18

1 Introduction

The TOTEM physics goals require the installation of new cylindrical shaped Roman Pots, which are radiofrequency optimized and are able to house timing detectors. The replacement of the present 147 m station is also necessary during LS1 to provide place for the installation of the TCL4 collimator. Both of these Roman Pot investigations may have an effect on the secondary production along the beam line, which can lead to known problems (increase in physics background, beam loss, ...). The main topic of this analysis note is to study the secondary production of the standard box and the new cylindrical shaped Roman Pots.

The studies and the results are based on Geant4 simulations. The Geant4 software and simulation environment is described in Section 2, where the two particle generators, used in the simulations, are also defined. Section 3 contains the studies involving only one Roman Pot: the box and cylindrical shaped Roman Pots are compared, where the different parts of the devices are tested separately to estimate their contribution. Beyond these relative comparisons a realistic study, based on a measured rate profile, is described in this section as well.

Section 4 includes the studies with two Roman Pots. Using this model avalanche effects can be estimated, for the box and cylindrical shaped Roman Pots.

2 Geant4 simulation environment

2.1 Physics list, production cuts

The version name of the Geant4 software, used for the simulation, is *geant4-09-06-patch-01*, which was released on 1/2/2013. The *QGSP_BERT 4.0* physics list is applied. The default production cuts are used which means that the same 700 μm cut is applied for each process.

2.2 Overall description of model geometry

The simulation consists of a particle generator, which generates the primary protons, one or two Roman Pots, depending on the scenario, and one register volume to report the secondary particles passing through a given area.

The position of the elements along the z-axis depends on the scenario as it is illustrated on Figure 1. The particle generator takes place at $z = 0$ m. The generated primary protons reach the first Roman Pot, whose center is placed at $z_{RP_1} = 0.15$ m. In multiple Roman Pot studies the center of the second Roman Pot is at $z_{RP_2} = z_{RP_1} + 4.6$ m. The produced secondary particles are registered with a register volume. In single Roman Pot studies the center of the register volume is at $z_{RP_1} + 6$ m. In multiple Roman Pot studies the position of the register volume center is $z_{RP_2} + 6$ m.

The transverse position of the elements depend on the concrete simulation, and these positions are given at the relevant point. The radius of the register volume is 100 km. It was chosen large enough to capture almost everything, even particles scattered under extraordinary large angle.

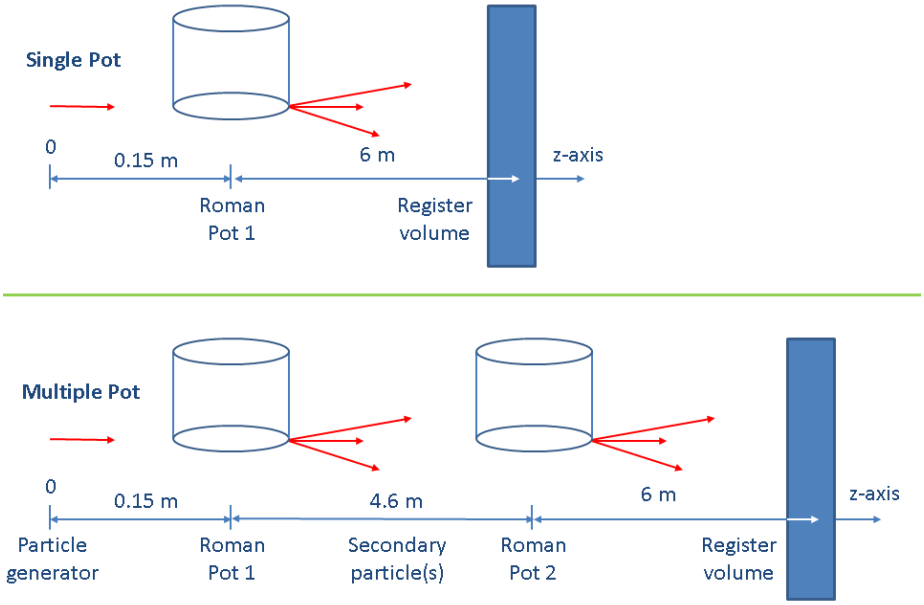

Figure 1: The position of the elements involved in the simulation along the z-axis. The particle generator takes place at $z = 0$ mm. The generated primary protons reach the first Roman Pot, whose center is placed at $z_{RP_1} = 0.15$ m. The produced secondary particles are registered with a register volume. In single Roman Pot studies the center of the register volume is at $z_{RP_1}+6$ m. In multiple Roman Pot studies the center of the second Roman Pot is at $z_{RP_2} = z_{RP_1}+4.6$ m and the position of the register volume center is $z_{RP_2} + 6$ m.

2.3 Particle generator definitions and purposes

2.3.1 δ-function profile

The purpose of this particle generator is to test the box and cylindrical shaped Roman Pots, by "shooting" their different parts with primary protons. In order to disentangle the beam optics contribution the distribution of the particles is singular, coming from one spatial point. In this way one can estimate the response of a given part in a clear way. With this information, theoretically, it is possible to estimate the response of a given pot with an arbitrary particle distribution.

With this generator $2 \cdot 10^3$ protons are produced in each simulation. The momentum components of the protons are $p_z = 7$ TeV/c and $p_x = p_y = 0$ TeV/c. This means that the protons are parallel with the z-axis. The position of the particle generator is $x_{\text{gen}} = z_{\text{gen}} = 0$ mm. The vertical position of the generator depends on the part which is under test, where the aim is to directly "hit" the tested piece. The possible combinations are collected in Table 1.

Pot part under study	y_{gen} [mm]
Bottom	0.05
Front thin window	20.0
Body	60.0

Table 1: The investigated parts of the two Roman Pots and the vertical positions of the particle generator, which were chosen such that the generated particles directly "hit" the tested part. In case of the bottom part the position is one third of the bottom foil thickness, see Table 7.

2.3.2 Profile based on measured rate

The δ-function profile described in the previous subsection is excellent to perform the relative tests of the different Roman Pot shapes. However, the Roman Pot rate measurements provide an outstanding opportunity to assemble a particle generator with a more realistic spatial distribution of particles.

In this case $6 \cdot 10^4$ protons are generated, with momentum components $p_z = 7$ TeV/c, $p_x = p_y = 0$ TeV/c as before. The particle generator position $z_{\text{gen}} = 0$ mm remains the same, but the distribution of the vertical positions y_{gen} is Gaussian, where $\sigma(y_{\text{gen}}) = 0.39$ mm, and the mean is 0 mm. This distribution corresponds to σ_y at $s = 220$ m using $\beta^* = 0.55$ m optics.

The horizontal positions x_{gen} are generated in a special way in the $[2, 90]$ mm interval, using a rate profile $R(x)$ measured by the 45 near horizontal Roman Pot of the TOTEM experiment at 220 m. The precise coordinates and properties of the measured rate data are given in Table 3 and the rate profile is plotted on Figure 3.

Each data point represents the rate measured by the whole detector surface. Therefore, the rate profile $R(x)$ can be treated as a convolution of a rate surface density profile $\rho(x)$, which describes the particle flow, and the detector surface:

$$R(x) \approx \int_0^l \rho(x+h)\omega(h)\, dh\,, \tag{1}$$

where l is the detector length measured along the detector center and $\omega(h)$ is the width of the silicon detector plane at position h. The shape and dimensions of the detector plane can be seen on Figure 2, where the interpretation of $\omega(h)$ is also shown.

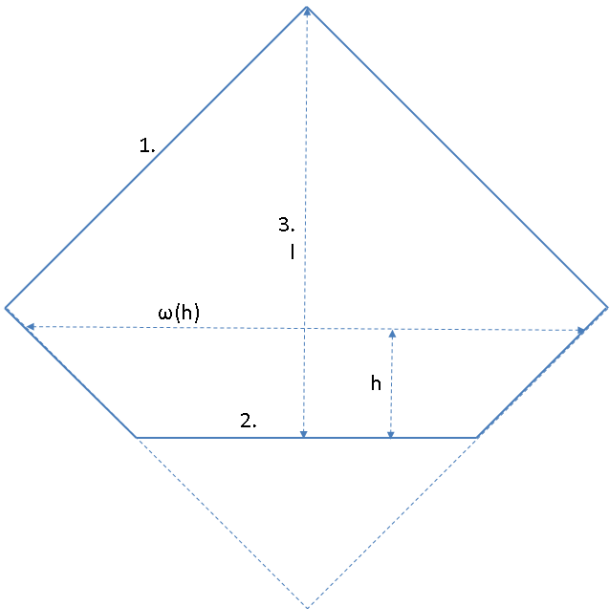

Figure 2: The shape and dimensions of the detector plane. The corresponding numbers are collected in Table 2.

Dimension	Value [mm]
1. Bounding rectangle edge	36.07
2. Length of detector edge	22.276
3. Length of detector (l)	39.872

Table 2: Dimensions of the diamond shaped register detector plane.

The rate profile $R(x)$ cannot be directly used in the generator since it is an integrated non-local quantity, instead the rate surface density $\rho(x)$ must be applied. Some assumptions are needed to do so: according to Figure 3 the domain of $R(x)$ can be divided to 3 distinct intervals with boundary points at 4.2 mm and at 21.5 mm. There is a break in the rate profile at each of these points, which must correspond to a jump or discontinuity in the rate surface density profile $\rho(x)$. The latter break point at 21.5 mm most probably corresponds to the collimator TCL5 while the source of the former is not yet understood.

Therefore, 3 Gaussian is used to build $\rho(x)$, one per each of these intervals:

$$\rho(x) = \begin{cases} g_1(x)\,, & 0.0 \leq x < 4.2\,, \\ g_2(x)\,, & 4.2 \leq x < 21.5\,, \\ g_3(x)\,, & 21.5 \leq x\,, \end{cases} \tag{2}$$

where

$$g_i(x) = c_i e^{-\frac{1}{2}\left(\frac{x-m_i}{\sigma_i}\right)^2}\,. \tag{3}$$

$\rho(x)$ is fitted using the convolution Eq. (1) to recuperate the rate profile $R(x)$. The result of the fit is shown with solid red line on Figure 3 and the fit parameters are collected in Table 4.

Property	Value
Filename	45_220_N_H.paw
Date	15/11/2012
Fill	3288
p/bunch	$1.6 \cdot 10^{11}$
Energy	4 TeV
β^*	0.6 m
ε_n	2.8 μmrad
μ	31

Table 3: The coordinates and properties of the rate measurement.

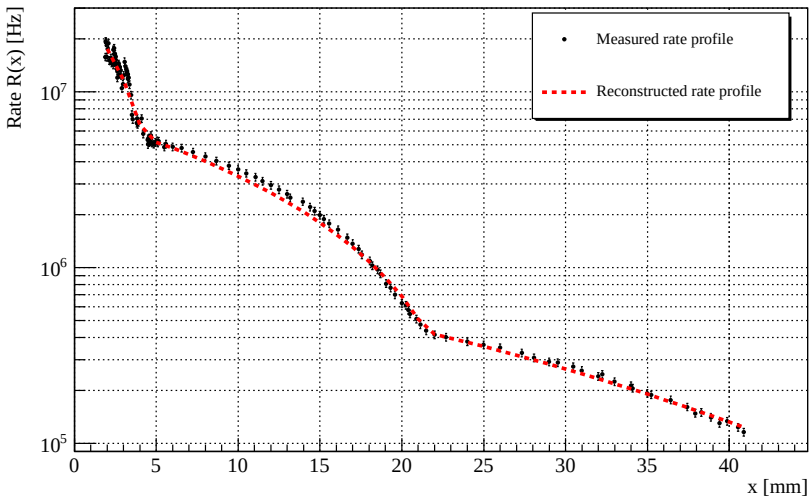

Figure 3: The measured rate $R(x)$ as a function of the distance of the Roman Pot bottom from the beam center. The data was taken by the 45 near horizontal Roman Pot at 220 m. The Roman Pot approached the beam step-by-step starting from parking position. Each data point represents the rate detected by the whole detector surface (the trigger rate) at that position. The red solid line shows the convolution Eq. (1) fitted to the data.

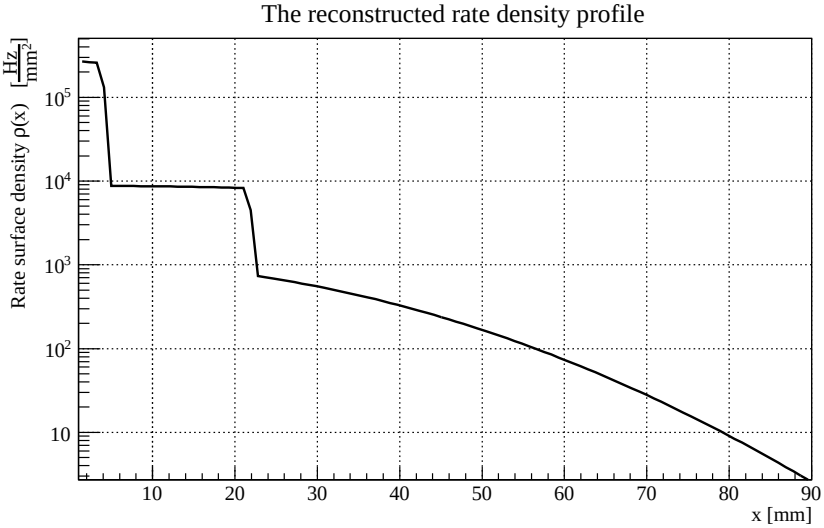

Figure 4: The reconstructed rate density profile $\rho(x)$. The function is a composition of three independent Gaussian whose interval and fitted parameters are given in Table 4.

i	Interval [mm]	c_i [Hz/mm^2]	m_i [mm]	σ_i [mm]
1	[0.0, 4.2)	$2.69 \cdot 10^5$	$4 \cdot 10^{-2}$	11.4
2	[4.2, 21.5)	$8.78 \cdot 10^3$	10^{-1}	60.0
3	[21.5, 90.0)	$1.08 \cdot 10^3$	10^{-1}	25.8

Table 4: Fit parameters of the rate surface density function Eq. (2). The three intervals correspond to the three intervals of $R(x)$, can be seen on Figure 3, which are separated by the location of the breakpoints in the rate profile.

Error	χ^2/ndf
5 %	3.0
10 %	0.8

Table 5: Fit quality parameters of Eq. (1), assuming 5% and 10% errors on the rate profile $R(x)$. The aim of this table is to demonstrate that the fit is compatible with some reasonable error assumption.

3 Single Roman Pot studies

3.1 Materials and geometries of the Roman Pots

3.1.1 Materials

The material of the Roman Pots is steel, AISI_316L_Steel, whose composition is described in Table 6. The description of the material was obtained from the TOTEM offline software, using the RP geometry description in the CMSSW framework.

Element	Fractional mass [%]
Iron	64.4
Chromium	18.0
Nickel	12.0
Molybdenum	2.5
Mangan	2.0
Silicon	1.0
Phosphor	$4.5 \cdot 10^{-2}$
Carbon	$3 \cdot 10^{-2}$
Sulfur	$3 \cdot 10^{-2}$

Table 6: The composition of the Roman Pot material, AISI_316L_Steel.

3.1.2 Standard Roman Pot

In this subsection the dimensions of the standard Roman Pot are given as it is described in the TOTEM offline software, using the RP geometry description in the CMSSW framework.

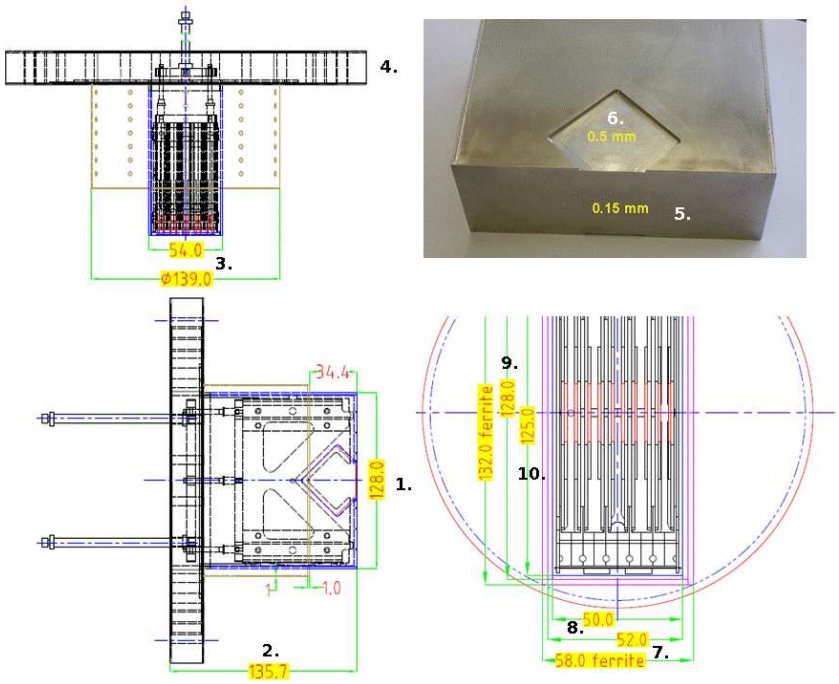

Figure 5: The relevant dimensions of the installed box shaped Roman Pot.

Dimension	Value [mm]
1. Boundary box x	128
2. Boundary box y	135.65
3. Boundary box z	54.0
4. Flange thickness	24.52
Height (2. - 4.)	115.15
5. Bottom foil thickness	0.15
6. Front thin window	0.5
Bottom wall thickness	2.0
7. Front wall + Secondary vacuum z	52.0
8. Secondary vacuum z	50.0
Front wall thickness (7. - 8.)	2.0
9. Front wall + Secondary vacuum x	128.0
10. Secondary vacuum x	125.0
Right, left wall thickness (9. - 10.)/2	1.5
11. Window size	37.71
12. Window center from bottom	14.16
13. Window bottom width	25.01

Table 7: Dimensions of the box shaped Roman Pot.

3.1.3 Cylindrical Roman Pot

In this subsection the dimensions of the cylindrical Roman Pot are given, where the values correspond to the production drawing received on 7/5/2013.

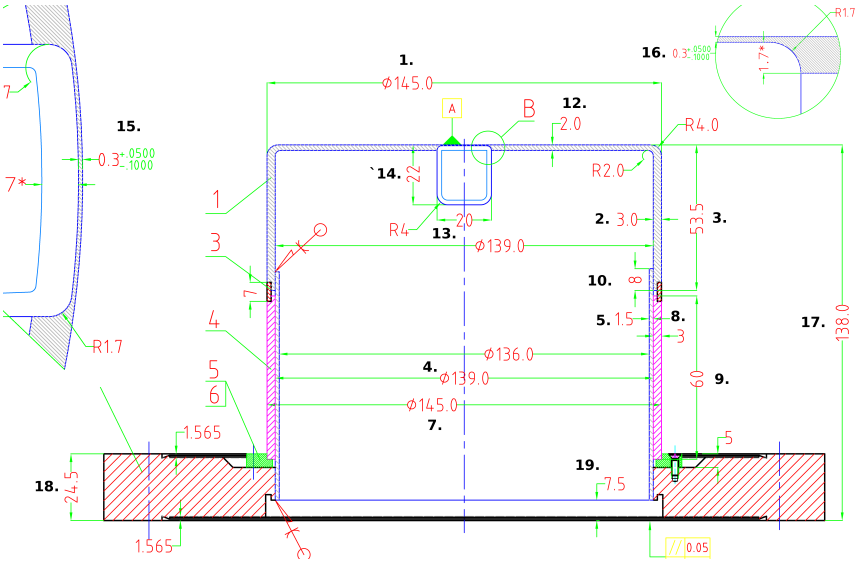

Figure 6: The relevant dimensions of the cylindrical Roman Pot.

Dimension	Value [mm]
1. Outer diameter lower part	145
2. Wall thickness lower part	3.0
3. Height lower part	53.5
4. Outer diameter upper part	139
5. Wall thickness upper part	1.5
6. Height upper part (17. - 3. - 19. + 10.)	85.0
7. Outer diameter ferrite	145
8. Thickness ferrite	3.0
9. Height ferrite (updated)	30.0
10. Shift upper lower part	8.0
11. Gap between ferrite lower part	2.0
12. Wall thickness bottom wall	2.0
13. Window width	20
14. Window height	22
15. Window thickness front	0.3
16. Window thickness bottom	0.3
17. Total height	138.0
18. Flange thickness	24.5
19. Distance flange upper part	7.5
20. Ferrite upper part distance	17.0
21. Height (6. + 3. - 10.)	130.5

Table 8: Dimensions of the cylindrical Roman Pot.

3.2 Secondary particle production

3.2.1 δ-function profile

In this section the secondary production of the standard box and cylindrical shaped Roman Pots are compared. The particle generator with δ-function profile is applied, which was defined in Section 2.3.1. The advantage of this generator that it does not contain any optics related parameters.

The longitudinal position of the Roman Pot is given on Figure 1. The center of the bottom boundary of the Roman Pot is at $x = y = 0$ mm.

The particle generator is directed to different parts of the Roman Pot one-by-one. The tested parts are: the bottom part, when the particle passes though the full material length of the bottom thin window. The thin window part, when the particle goes through on the thin window only. And the "body" part, when the particle trajectory goes through the wall over the thin window, testing the full wall thickness. The concrete positions are given in Table 1.

In case of the standard box shaped and cylindrical Roman Pot the particles generated by the bottom part are shown on Figure 7. The scatter plots show the secondary particles detected by the register volume which is placed after 6 m the Roman Pot. To provide a scale the beam pipe is indicated on the Figure with a white circle with 40 mm radius around the origin.

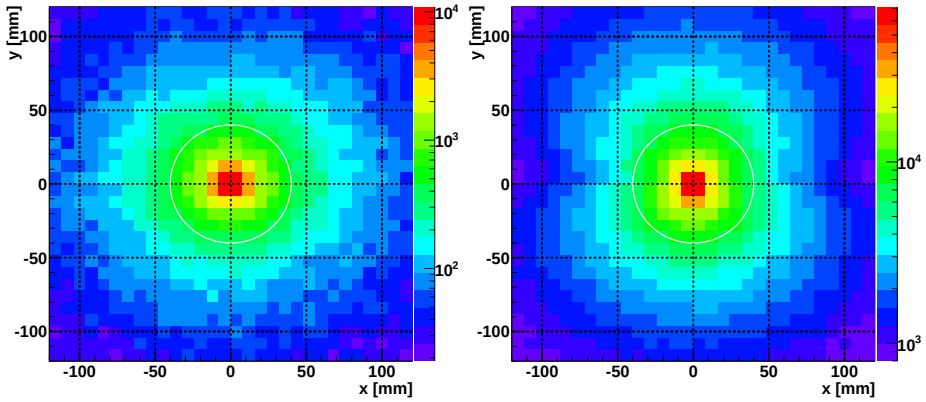

Figure 7: Distribution of the secondary particles created by the bottom foil of a standard box shaped Roman Pot (left) and a cylindrical Roman pot (right). The secondary particles are registered by the register volume 6 meters farther. The particle generator is described in the text as δ-function profile generator. The white circle around the origin with radius 40 mm indicates the beam pipe. According to the scales of the plots the cylindrical Roman Pot induces 5-6 times more secondary particles.

To describe and quantify the distribution of the secondary particles, their scattering angle distribution, horizontal and vertical, is fitted with the following function:

$$\rho(\Theta_x) = C \cdot \left(\frac{\Theta_x - b}{d} \right)^{-a}, \tag{4}$$

where $d = 1$ mrad.

This function provides a reasonable description of the results. The result of the fits in case of the horizontal scattering angle Θ_x distributions are shown on Figure 8 and the obtained fit parameters are collected in Table 9. The results in case of the vertical scattering angles Θ_y can be seen on Figure 9 and the corresponding parameters are collected in Table 10.

It was found that the fits, obtained with Eq. (4), are good approximations down to about 0.1 mrad scattering angles. This scattering angle corresponds to a displacement with 0.6 mm after 6 meters.

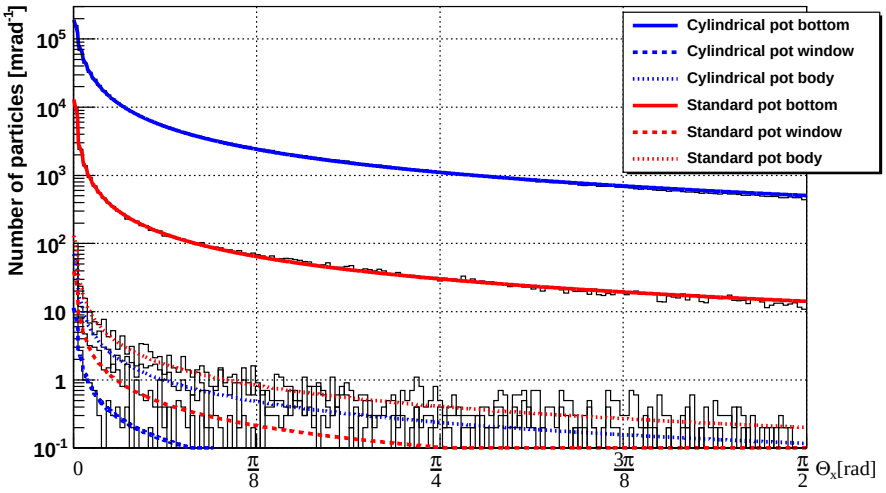

Figure 8: The horizontal scattering angle Θ_x distribution of secondary particles produced by different parts of the standard box shaped Roman Pot and by the cylindrical Roman Pot. The graph of the fits with function Eq. (4) is also shown. The fit parameters are collected in Table 9. The bin width is 10 mrad, which is approximately $\Delta x = 60$ mm on Figure 7.

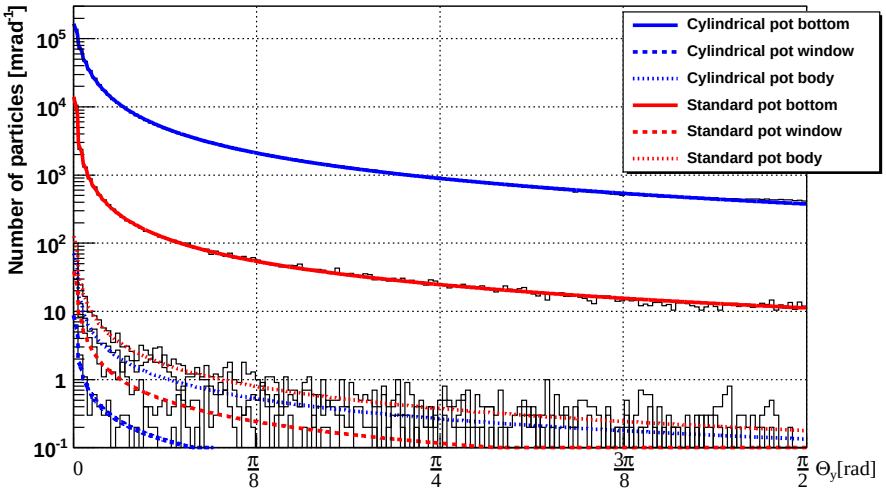

Figure 9: The vertical scattering angle Θ_y distribution of secondary particles produced by different parts of the standard box shaped Roman Pot and by the cylindrical Roman Pot. The graph of the fits with function Eq. (4) is also shown. The fit parameters are collected in Table 10.

Shape	Bottom			Window			Body		
	C [mrad^{-1}]	a	b [mrad]	C [mrad^{-1}]	a	b [mrad]	C [mrad^{-1}]	a	b [mrad]
Cylindrical	$8.47 \cdot 10^5$	1.13	-5.04	23.0	1.07	1.07	185	1.02	1.10
Standard	$2.32 \cdot 10^4$	1.09	1.14	79.3	1.05	1.42	318	1.02	1.42

Table 9: The horizontal scattering angle Θ_x distribution of secondary particles produced by different parts of the standard box shaped Roman Pot and by the cylindrical Roman Pot is parametrized with function Eq. (4). The parameters of the fits are collected in this table.

Shape	Bottom			Window			Body		
	C [mrad^{-1}]	a	b [mrad]	C [mrad^{-1}]	a	b [mrad]	C [mrad^{-1}]	a	b [mrad]
Cylindrical	$6.69 \cdot 10^5$	1.26	-9.41	28.8	0.92	2.26	209	0.98	1.51
Standard	$1.87 \cdot 10^4$	1.13	1.27	90.3	1.05	1.07	289	1.07	0.59

Table 10: The vertical scattering angle Θ_y distribution of secondary particles produced by different parts of the standard box shaped Roman Pot and by the cylindrical Roman Pot is parametrized with function Eq. (4). The parameters of the fits are collected in this table.

3.2.2 Profile based on measured rate

In this section the "realistic" particle generator is applied, which is based on a measured rate, described in section 2.3.2. The measurement was done by a horizontal Roman Pot, hence in the simulation a standard horizontal Roman Pot is placed, where the positions of the elements along the z-axis are indicated on Figure 1. The center of the bottom boundary of the Roman Pot is vertically at $y = 0$ mm and horizontally at $x = 2$ mm, in order to be compatible with the smallest x-coordinate of the measured data, $R(x)$.

The response of the horizontal Roman Pot for the generated particle input can be seen on Figure 10, where as usual the secondary particles detected by the register volume 6 meters farther are plotted. The beam pipe is indicated with a white circle around the origin.

If the number of secondary particles inside the beam pipe N_{pipe} is divided by the total number of secondary particles N_{all} detected by the register volume

$$\frac{N_{\text{pipe}}}{N_{\text{all}}} = \frac{1.9 \cdot 10^5}{7.5 \cdot 10^5} \approx 25.4\,\%\,, \tag{5}$$

one can see that 25.4 % of the secondary particles remain in the beam pipe at 6 meters.

A plot about the flow of the total energy, carried by the secondary particles, is also included on Figure 11. The corresponding numbers for the total energy

$$\frac{E_{\text{pipe}}}{E_{\text{all}}} = \frac{8.4 \cdot 10^6 \text{ GeV}}{9.3 \cdot 10^6 \text{ GeV}} \approx 91.0\,\%\,, \tag{6}$$

show that the energy is even more forward directed than the secondary particle flow

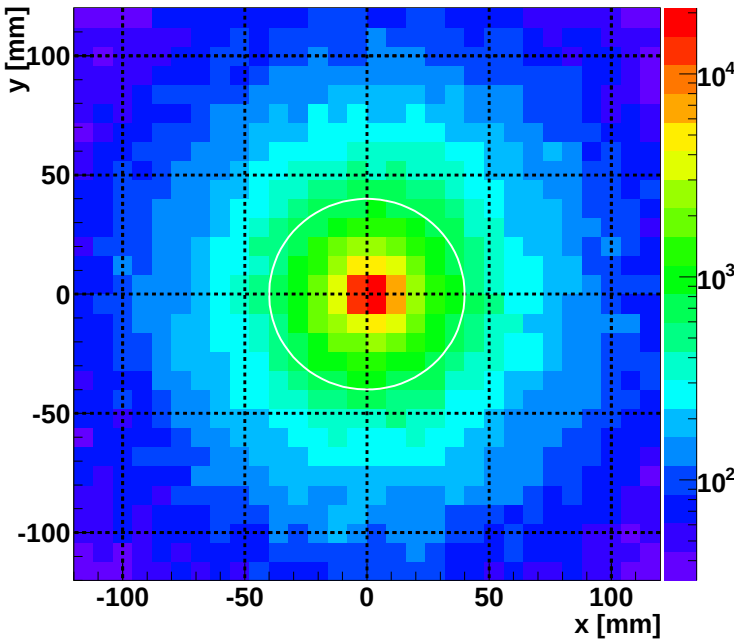

Figure 10: Distribution of the secondary particles created by the horizontal standard box shaped Roman Pot and registered by the register volume 6 meters farther. The particle generator is based on the measured rate profile. The white circle around the origin with radius 40 mm indicates the beam pipe.

The rate data is given in Hz, and according to Figure 3 around $1.5 \cdot 10^7$ particles are detected in each second at 2 mm. The simulation contains only $6 \cdot 10^4$ particles, which means that in order to scale the result of Figure 10 to a Hz level, a normalization factor have to be applied.

To give the correct normalization one sensitive detector plane was included into the simulation, and was placed into the pot. The shape of the detector plane is identical with the installed diamond shaped silicon detector plane of the Roman Pots, see Figure 2, but its material is vacuum being only a register volume. The relevant dimensions are given in Table 2.

The register detector is placed at $z = 0$ mm in the Roman Pot local coordinate system, which is the longitudinal center of the Roman Pot. The distance between the detector edge and the bottom foil is 200 μm, following the dimensions of the TOTEM offline software geometry in the CMSSW framework.

In total 51687 primary protons were detected by the register detector plane. As it was mentioned, following Figure 3, in reality around $1.5 \cdot 10^7$ particles are detected at 2 mm per second. Therefore the multiplication factor to obtain Hz is around 290.2 Hz.

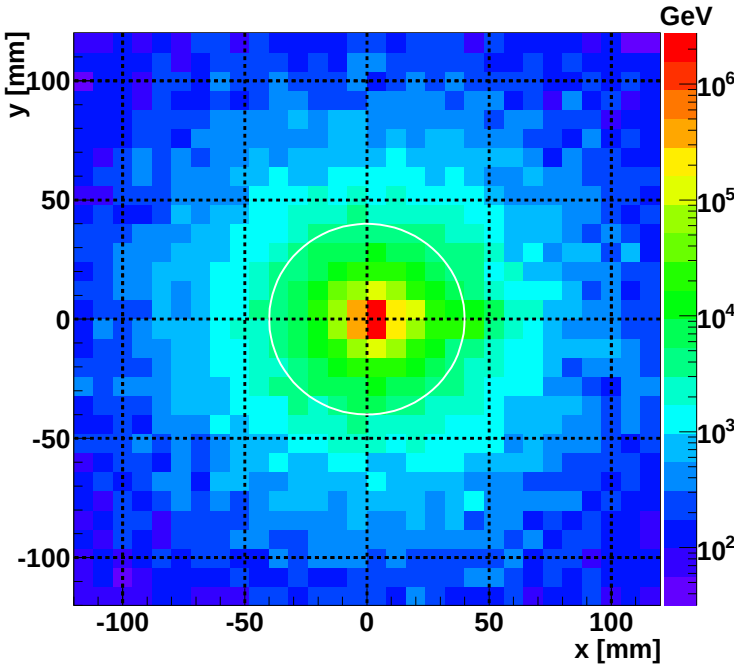

Figure 11: Distribution of the total energy flow carried by the secondary particles created by the horizontal standard box shaped Roman Pot and registered by the register volume 6 meters farther. The particle generator is based on the measured rate profile. The white circle around the origin with radius 40 mm indicates the beam pipe.

3.3 Conclusions

It was found that the angular distribution of the secondary particles can be described reasonable with a Θ^{-1} angular dependence. The success of this parametrization already proves that the particle flow is very forward. A direct test shows that 25.4 % of the secondary particles remain in the beam pipe at the register volume which is placed 6 meters farther. Moreover, at the same position, 91.0 % of the total energy flow is contained by the beam pipe.

The parametrization Eq. (4) allows us to approximately quantify the relative contribution of the different pots and also their parts. The results described in Table 8 and 9 clearly show that the bottom part is the main source of secondary production, and the relative contribution with respect to other parts is:

$$C_{\text{bottom}} > 50 \times C_{\text{other}}. \tag{7}$$

The same results show, that more secondary particles are produced by the cylindrical pot than by the standard box:

$$C_{\text{cylindrical,bottom}} > 10 \times C_{\text{box,bottom}}. \tag{8}$$

The horizontal and vertical angular distributions are very similar.

4 Multiple Roman Pot studies

4.1 Secondary particle production

4.1.1 δ-function profile

In this section the secondary production of two subsequent standard box and cylindrical shaped Roman Pots are studied. The particle generator with δ-function profile is applied. Figure 1 shows the arrangement of the two Roman Pots and the position of the register volume.

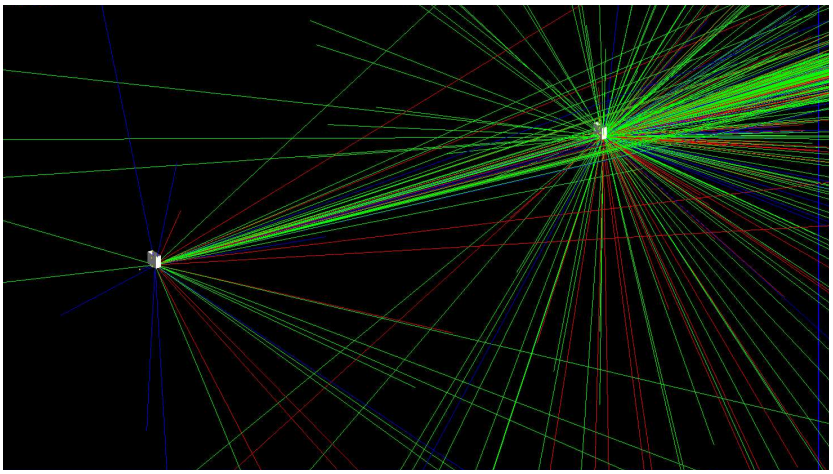

Figure 12: Event display illustrating the avalanche effects in case of two subsequent box shaped Roman Pots.

The scatter plots of the detected secondary particles are shown on Figure 13. According to these results in case of the box shaped Roman Pots an increase by a factor of 2 can be observed, with respect to the single Roman Pot case, Figure 7. In case of the cylindrical Pots a shadowing effect can be observed in the horizontal plane, due to the longer path in the bottom foil. Consequently the avalanche effects are suppressed.

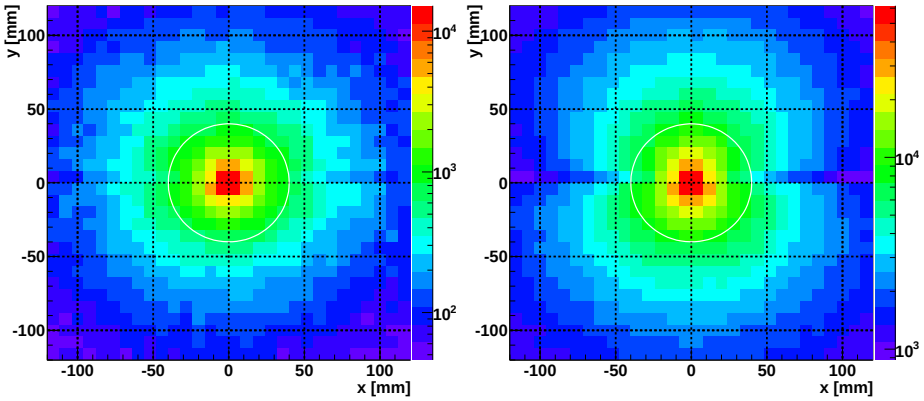

Figure 13: Distribution of the secondary particles created by two subsequent standard Roman Pots (left) and cylindrical ones (right), where the register volume is placed after the second pot with 6 meters, according to Figure 1. The particle generator is described in the text as δ-function profile generator and it is directed to the bottom part of the first Roman Pot. The white circle around the origin with radius 40 mm indicates the beam pipe. According to Figure 7 an increase in the number of secondary particles by a factor of 2 can be observed in case of the standard box shaped Roman Pots. In case of the cylindrical Roman Pots a shadowing can be observed in the horizontal plane, and the avalanche effects are less obvious.

4.1.2 Profile based on measured rate

According to the Roman Pot measurements the rate detected by the far horizontal Roman Pot is higher than the rate detected by the near one. The measured ratio $\mathcal{R}_{\text{measured}}$ when the distance of the Roman Pot from the beam is 2 mm:

$$\mathcal{R}_{\text{measured}} = \left.\frac{R_{\text{far}}(x)}{R_{\text{near}}(x)}\right|_{x=2\text{ mm}} \approx 3.5\,. \tag{9}$$

To understand the source of this increase, in the simulation the number of charged particles detected by the silicon detector plane of the far pot is divided by the corresponding number detected by the near pot:

$$\mathcal{R}_{\text{simulated}} = \frac{N_{(\text{charged, far})}}{N_{(\text{charged, near})}}\,. \tag{10}$$

The results are collected in Table 11. The results show that the source of the increase is partially the secondary particles produced by the first Roman Pot, but according to Table 11, a lot of secondary particles are created *inside* the second device.

4.2 Conclusions

The multiple Roman Pot studies confirmed the presence of avalanche effects. Using the register volumes an increase by a factor of 2 can be observed in the

	Detector at		
	front	middle	back wall
$\mathcal{R}_{\text{simulated}}$	1.5	1.8	2.5

Table 11: The simulated ratio $\mathcal{R}_{\text{simulated}}$, and its dependence on the position of the detector plane *inside* the far Roman Pot.

secondary particle production after the second Roman Pot with respect to the first one.

According to the simulation a relevant part of the secondary particles detected by the second Roman Pot is created inside the second Roman Pot.